Response of water-biochar interactions to physical and biochemical aging

Asier Goñi-Urtiaga, Denis Courtier-Murias, Giuseppe Picca, Juan L. Valentin, César Plaza, Marco Panettieri

Response of water-biochar interactions to physical and biochemical aging

Asier Goñi-Urtiaga[1], Denis Courtier-Murias[2], Giuseppe Picca[1], Juan L. Valentin[3], César Plaza[1] and Marco Panettieri[1]*

[1] Instituto de Ciencias Agrarias, Consejo Superior de Investigaciones Científicas (ICA-CSIC), Calle Serrano 115bis, 28006 Madrid, Spain

[2] Univ Gustave Eiffel, GERS-LEE, F-44344 Bouguenais, France

[3] Instituto de Ciencias y Tecnología de Polímeros, Consejo Superior de Investigaciones Científicas (ICTP-CSIC), Calle Juan de la Cierva 3, 28006 Madrid, Spain

* Corresponding author marco.panettieri@csic.es

Abstract

Biochar aging may affect the interactions of biochar with water and thus its performance as soil amendment; yet the specific mechanisms underlying these effects are poorly understood. By means of FTIR, N_2 adsorption, Hg intrusion porosimetry, thermogravimetric analysis, ^{13}C solid state nuclear magnetic resonance (NMR) and ^{1}H NMR relaxometry, we investigated changes in the chemistry and structure of biochar as well as its interaction with water after biochar aging, both physical (simulated by ball-milling) and biochemical (simulated by co-composting). Three different porosities of biochar were examined: <5 nm, 1 µm and 10 µm diameter sizes. Physical aging caused the disappearance of the porosity at 10 µm. With biochemical aging, biochar underwent an enrichment of oxygenated functional groups either as a result of surface functionalisation processes or by the deposition of fresh organic matter layers on the surface and pores of biochar. ^{1}H NMR relaxometry revealed that the proportion

of water strongly interacting with biochar increased with both physical and biochemical aging. Although biochemical aging significantly altered the composition of biochar surface and modulates its interaction with water, ^{1}H NMR relaxometry proved that physical aging had a relatively stronger influence on water mobility and dynamics in biochar, lowering both T_1 and T_2 relaxation times in the initial contact times of biochar and water.

Keywords

Biochar; Aging; Co-composting; NMR Relaxometry; Water interactions; Porosity.

Introduction

In the last decades, the interest in the use of biochar as soil amendment has greatly increased. Biochar is a carbonaceous material derived from the pyrolysis of biomass with great potential for carbon sequestration while improving soil fertility [1,2]. During the pyrolysis process to produce biochar, the biomass feedstock loses most of its labile organic matter leading to a chemically stable and porous material with a considerably high degree of condensed aromatic rings. Biochar has an estimated residence time of hundreds of years when applied to soils [3] but during degradation suffers chemical and physical alterations, a process known as biochar "aging" [4-6]. The characteristics of biochar, its interactions with plants, water and soils, and its persistence within soils depend on the feedstock of biomass and on the temperature and residence time of the pyrolysis process [7,8].

In recent years, the combination of compost and biochar has been proposed to obtain a fertile mixture for soil amendment. The addition of biochar to compost improves the performance of the composting process, increasing the temperature and duration of the thermophilic phase by the enhancement of microbial activity and capturing potentially toxic metals and organic compounds [9,10]. During co-composting, biochar undergoes surface modifications by the addition of surface functional groups which increases its cationic exchange capacity (CEC) and

52 interaction with other chemical compounds present in soil, facilitating nutrient retention as
53 well as acting as a pH buffer [11]. Besides, the high porosity of biochar provides large specific
54 surface area which can greatly improve water holding capacity in soils or plant-growing media
55 [12], maintaining desired moisture and promoting the aforementioned nutrient retention.
56 Some biochar modifications during co-composting are produced by biochemical processes
57 driven by microbial decomposition of organic matter. As reported by Wang et al. (2020), this
58 can produce an enrichment of oxygenated functional groups on its surface. Besides, they
59 consider that biochar aging within composting piles and within soil after application should be
60 driven by similar biochemical reactions leading to similar aged biochars, but on a different
61 timescale considering co-composting process as a way to accelerate biochar aging [4,13]. Some
62 authors proposed that, during this biochemical aging taking place in biochar, a layer of fresh
63 organic matter is formed on the surface of biochar particles and pores, which creates a
64 chemically reactive and nutrient-rich material with beneficial properties for soil fertilisation
65 and plant growth [14,15]. To comprehend the mechanism concerning the benefits of aged
66 biochar and the effect on plant-biochar interactions modulated by water holding capacity and
67 nutrient release to the rhizosphere, the role of water interactions in the biochar particles must
68 be understood.
69 Physical fragmentation is another aging mechanism that may affect biochar porosity, particle
70 size and accessibility to inner porosity, which are key to water holding capacity and water
71 interactions in biochar. This physical aging (or disruption) is caused by soil weathering,
72 freeze/thaw temperature cycles and by tillage with agricultural machinery [4]. However, it
73 occurs during long time spans, thus for this study we used ball milling of biochar to reduce
74 particle size, which roughly led to a comparable effect as physical weathering (aging) of
75 biochar in the field. Several authors stated that water retention is mainly dependent on the
76 porosity and particle size of biochar [17,18], proposing different mechanisms where inter-
77 aggregate porosity (between particles), intra-aggregate porosity (structural pores), zeta

potential or poly-condensed carbon ring interaction by H-bonds play the main role in water retention.

Thus, a number of studies of literature show that both biochemical and physical aging are key parameters on the modulation of water holding capacity of biochar but their relative importance is still unknown [19]. Most of these studies are based on biochars produced from different feedstock materials or pyrolysis conditions, which also affect physical and chemical properties of the final product and, thus, water retention [20]. Moreover, the information on water interactions concerning biochar aged in composted piles or in soils, where the interaction between water and functionalised surface of the material should change compared to that of pristine biochar, mainly deals with quantification or macro-scale processes, while processes at smaller scales are unaddressed [4]. In the present investigation, the effects of physical and biochemical aging on the chemical properties of biochar and its interactions with water were investigated. FTIR, porosimetry analysis, ^{13}C solid state nuclear magnetic resonance (NMR) and thermogravimetric analysis (TGA) were used to examine the chemical modification of biochar after physical aging (simulated by ball-milling) and during biochemical aging (simulated by co-composting). This information was used in combination with 1D ^{1}H NMR relaxometry and, for the first time, with 2D ^{1}H NMR relaxometry to study water dynamics (i.e. molecular tumbling) in the different pores of biochar at the molecular scale.

There are several examples of ^{1}H NMR relaxometry (i.e. study of NMR relaxation) applications in porous media in general such as wood, concrete, clay, etc [21-23]. Concerning wood/lignocellulosic samples, the technique has already been used for some decades [24] but it is gaining popularity in recent years due to the development of low-cost (and -maintenance) low-field NMR spectrometers. These instruments allow to perform time domain (TD)-NMR experiments to obtain NMR relaxation information but can also obtain 1D MRI profiles [25] and diffusion information [26]. NMR relaxometry allows to study wood materials under different conditions (non-invasively) to quantify water or organic molecules and to obtain

104 information regarding their local environment (i.e. pore size, affinity with molecules/surfaces
105 they are bonded to). The major part of this research focused on studying water adsorbed on
106 the wood's walls using 1D NMR relaxometry. For instance, Sharp et al. [27] studied wood's
107 moisture content (MC) and other related studies quantified bound water and free water
108 contents by spin-spin (T_2) NMR relaxation time measurements [28–32]. In addition, by means
109 of T_2 NMR measurements Araujo et al. (1994) focused on the separation of hydration and
110 solution water [33]. Recently, Cox et al. (2010) and Bonnet et al. (2017) have used 2D NMR
111 relaxometry experiments via spin lattice (T_1)-T_2 correlation [34, 35]. This better separate water
112 components detecting two types of bound water in wood cell-wall, which were not
113 differentiated in 1D experiments. Cox et al. also studied liquid water in the lumen, which was
114 identified as the peak with the highest T_1 and T_2 values and being close to the T_1=T_2 line. This
115 technique has also been used to study biomass recalcitrance in the presence of liquid water
116 [36]. Based on these previous works, the current study thus provides a characterization of
117 water-biochar interactions under aging simulated conditions, to optimize the use of biochar for
118 fertility enhancement and carbon sequestration under environmental conditions.
119
120 **Materials and methods**
121 *Biochar, biochemical and physical aging, and sampling*
122 Biochar produced from the pyrolysis of pine *(Pinus Halepensis)* prune using a low-tech Kon-tiki
123 oven with a high heating temperature (HTT) of 650-750 °C and a residence time of 3-3.5 h was
124 obtained from *Carbón Vivo, SCCL (Barcelona, Spain)*. The pyrolysis conditions (i.e. the absence
125 of oxygen) are assured by the fire curtains created on top of the material in the Kon-tiki oven
126 and quenching was carried out watering the oven from the top using approximately twice the
127 volume of water than the oven capacity. Biochemical aging of biochar was achieved co-
128 composting a mixture of prune, spent coffee grounds and biochar (1:1:1 v/v) in a 200 L
129 composter during 30 days under monitored temperature (Figure SI-3) and 40-60% humidity

conditions. A composite sample of about 500 g of the mixture was collected after 0, 9 and 30 days from five random points (≈ 100 g per point) within the composting pile and mixed together to assure the homogenization of the sample. Biochar particles were separated by hand from the composite samples using tweezers and selecting ≥2 mm diameter composted particles. A portion of the samples were ground with a ball mill for 10 min at a frequency of 25 s^{-1} to simulate physical aging and for physicochemical characterization. Samples were labelled as unaged biochar (BC), physically aged biochar (pa-BC), biochemically aged biochar (ba-BC), and physically and biochemically aged biochar (pba-BC).

Physicochemical characterisation

Particle size was measured using a Mastersizer 3000 laser diffraction particle size analyser (Malvern Panalytical). Fourier transformed infrared spectroscopy (FTIR) was performed in a FTIR-8400 Shimadzu spectrometer [37]; samples were prepared by grinding 1 mg of biochar materials (previously dried at 105 °C, 24 h) with 200 mg KBr and pressing into a pellet. Infrared spectra were recorded in a wavenumber range of 450 – 4000 cm^{-1}. TGA was carried out in a Setaram SETSYS 16/18 TGA-ATD analyser [38] under He and synthetic air atmospheres in a temperature range of 25 – 900 °C and 10 $K \cdot min^{-1}$ heating ramp; 20 mg of the sample was weighted in an alumina crucible for the measurement. Porosity was measured using two different methods targeting micro and macro porosity using N_2 adsorption and Hg intrusion, respectively. N_2 adsorption porosimetry was determined using a Quantachrome Autosorb AS-1 instrument [39]. Briefly, biochar samples were degasificated at 150 °C and biochemically aged biochar samples at 105 °C (to avoid thermal decomposition of labile matter), both for 20 h in vacuum conditions. Surface area and pore size distribution were obtained using Brunauer-Emmett-Teller (BET) and Barrett–Joyner–Halenda (BJH) methods, respectively, using AS1-Win software. Hg intrusion porosimetry was carried out with a AutoPore IV 9510 Micromeritics equipment with a pore size resolution between 0.1 and 360 µm [40]. ^{13}C solid state NMR

156 measurements were performed using a cross-polarization sequence at the magic angle
157 spinning (CP-MAS) [41] in a 400 MHz Bruker Advance III spectrometer, using a 4 mm zirconia
158 rotor, 13 kHz spinning speed. A ramped ^{1}H-pulse from 100 to 50% of the full power was used
159 during a contact time of 1 ms to reduce Hartmann-Hahn mismatches and 500 ms recycle delay
160 between scans. A contact time of 1 ms is frequently used to obtain an efficient coupling
161 between protons and ^{13}C atoms in environmental samples rich in aromatic rings, such as
162 biochar, as a compromise for a good polarization for the different organic components [41,
163 42]. The obtained spectra were divided in six regions contributing to the total measured ^{13}C
164 intensity and corresponding to the carbon atoms in the following functional groups: alkyl (0-45
165 ppm), *N*-alkyl/mehoxyl (45-60 ppm), *O*-alkyl (60-90 ppm), anomeric (90-110 ppm), aryl (110-
166 140 ppm), heteroaromatic (140-160 ppm) and carboyl/amide (160-220 ppm) [43,44].
167 FTIR, TGA-DSC and particle size analysis were performed on triplicate samples. For ^{13}C NMR
168 and porosimetry, to reduce experimental time and costs, analyses were performed on one
169 composite sample per treatment.
170
171 *Measurements of water-biochar interactions using ^{1}H NMR relaxometry*
172 Three different levels of water content were set up for all biochar samples. Firstly, dry samples
173 were wetted with an excess of deuterated water (D_2O) to increase the mobility of structural
174 hydrogen atoms and hence to increase their relaxation time signal without adding hydrogens
175 from water. This way, it is possible to evaluate the structural proton NMR signal from biochar
176 at the experiment conditions and its effect on the subsequent measurements with water
177 (H_2O). Secondly, samples were placed in different desiccators for 5 days in specific relative
178 humidity (RH) controlled by a saturated solution of salt; $Mg(NO_3)_2$ (RH=55%), NaCl (RH=75%)
179 and pure water (RH=100%), to prepare samples with adsorbed but not free water. Finally, all
180 samples were mixed with deionized water in a 1:4 mass ratio for liquid water analysis.

^{1}H relaxometry measurements were carried out in a low field (0.5 Tesla) Bruker Minispec mq20 spectrometer. About 80 mg of sample was weighted for each sample and placed in 8 mm diameter glass tube. Temperature was controlled by a BVT3000 temperature controller with air flow of 1200 L h^{-1} at 30 °C for all measurements. Samples were maintained at these conditions for 30 min before each measurement to ensure temperature control. Transverse NMR relaxation times (1D T_2) were estimated using the Carr-Purcell-Meiboom-Gil (CPMG) sequence [45,46], using the following test variables (i) for controlled % RH samples: 0.08 ms echo time repeated 625 times, 1 s recycle delay and 96 scans and (ii) for samples with liquid water: 0.5 ms echo time repeated 10000 times, 10 s recycle delay and 96 scans. The obtained data was treated with CONTIN-based home-made method, as reported in previous work [47] to obtain 1D T_2 distributions.

Finally, 2D NMR correlation spectra of longitudinal (T_1) and transverse (T_2) relaxation times were obtained using a coupled sequence of Inversion Recovery and the CPMG. For the Inversion Recovery experiments, the delay was increased logarithmically in 48 steps from 0.01 to 3000 ms. The CPMG block utilised an echo time of 0.5 ms, among which 300 echoes where recorded following a logarithmic series from 0.5 to 1000 ms. For this 2D sequence, 4 scans were accumulated with a recycle delay of 5 s. T_1-T_2 correlation spectra were calculated using an in-house software, reproducing 2D-inverse Laplace transform (ILT) algorithm [48]. For further information, refer to Bonnet et al. 2017 [35] and Rostom et al. 2019 [49].

In general, 1D T_2 NMR relaxometry is used to distinguish bound and free water (being the main advantage a short experimental time lasting few minutes) and 2D T_1T_2 correlation NMR relaxometry to improve resolution and obtain physical and chemical information on the samples [50]. Concerning data interpretation, the area under each peak of either 1D or 2D spectra is proportional to the amount of H atoms and thus water molecules. 1D spectra will allow to quantify the amount of water in different environments. For 2D spectra, the T_1 and T_2 NMR values of each peak give unambiguous access to T_1-T_2 ratios. This is characteristic of H

207 atoms mobility and confinement and greatly helps spectrum interpretation. Depending on the
208 value of these ratios, water can be identified as unconfined water, mobile free water, mobile
209 adsorbed water, and immobile water molecules bonded to solid macromolecules. Ratios lower
210 than one are physically not permitted [51].
211 For readers interested on this technique, let us briefly explain more about the influence of
212 water mobility and environment on the relaxation times T_1 and T_2 but cited references should
213 be consulted for detailed information. T_1 and T_2 NMR values depend on the local environment
214 of the measured hydrogen atoms (H). In this case this will correspond to water molecules and
215 their NMR relaxation values will depend on the size of the molecules they are bound to,
216 affinity with molecules interacting and pore size. T_2 NMR relaxation times decreases as pore
217 size is reduced (increase of surface-to-volume ratio) and/or when molecular tumbling (internal
218 mobility) decreases. They will also decrease if H atoms are in molecules with restricted
219 mobility due to viscosity, or the interactions being in macromolecules. For T_1 NMR relaxation
220 times, first they will decrease when molecular tumbling decreases (from liquid phase) but it
221 increases when molecular tumbling is low (in gel and solid like molecules) [49]. Here is where
222 we can see the importance of T_1-T_2 ratios, which are characteristic of the mobility of H atoms
223 and will provide physical information of water. Values close to 1, 2–6, and over 10 have been
224 assigned to (i) unconfined water, (ii) mobile water at free or adsorbed state and (iii) bonded
225 immobile water molecule and solid macromolecules, respectively [35]. These values may vary
226 depending on the system studied but the trend in the increase of T_1-T_2 should be valid for any
227 material.
228
229 **Results**
230 *Physicochemical properties of biochar*
231 The FTIR spectrum of unaged biochar (BC) exhibits weak bands at 3400 cm^{-1} (mainly due to O-
232 H stretching) and at 2900 cm^{-1} (due to aliphatic C-H stretching). Relatively stronger bands were

found at 1600 cm^{-1} (attributed to C=C and C=O stretching of conjugated ketones and quinones), at 1050 cm^{-1} (corresponding to C-O stretching likely from non-decomposed lignocellulosic materials), and at 1400, 885 and 775 cm^{-1} (corresponding to C-H_2, aromatic C-H and aromatic out-of-plane C-H stretching, respectively), characteristic of samples with a high degree of C condensation *(Figure 1)*. The absorption at 3400 cm^{-1} increases with the time of biochemical aging (co-composting), indicating an increased presence of hydroxyl and carboxyl groups. Similarly, the intensity of the signal at 2900 cm^{-1} increases with time of biochemical aging, suggesting an increased contribution of signals from microbial lipids and/or persistent vegetal lipids.

According to solid state NMR data *(Figures 2 and SI-1)*, unaged biochar exhibits a high content of aromatics (55.0% of the total C intensity measured) relative to other types of carbon. After 9- and 30 days of biochemical aging, the contribution of *O*-alkyl and alkyl groups increases (from 5.5 to 11.0% and from 7.0 to 10.2%, respectively). The intensity of the aromatic carbon signal is similar for unaged and biochemically aged biochar, indicating that the separation process of biochar particles from the compost mixture, as referred in *Materials and Methods,* is highly efficient.

All samples exhibit an initial mass loss of 4% with heating below 110 °C corresponding to adsorbed atmospheric humidity *(Figure 3)*. In inert atmosphere, thermal decomposition of BC starts at 350 °C, with a 6% mass loss below 680 °C and a 5% mass loss at temperatures above 680 °C. An additional mass loss of 11% is appreciated in ba-BC above 250 °C, corresponding to the modification of biochar with a labile organic fraction or to surface functionalities during co-composting. In the presence of air atmosphere, mass loss above 250 °C is similar, and ba-BC underwent a 9% loss from oxidation. Both samples exhibit a high final residue of ~30% corresponding to ash and remnants of high recalcitrance.

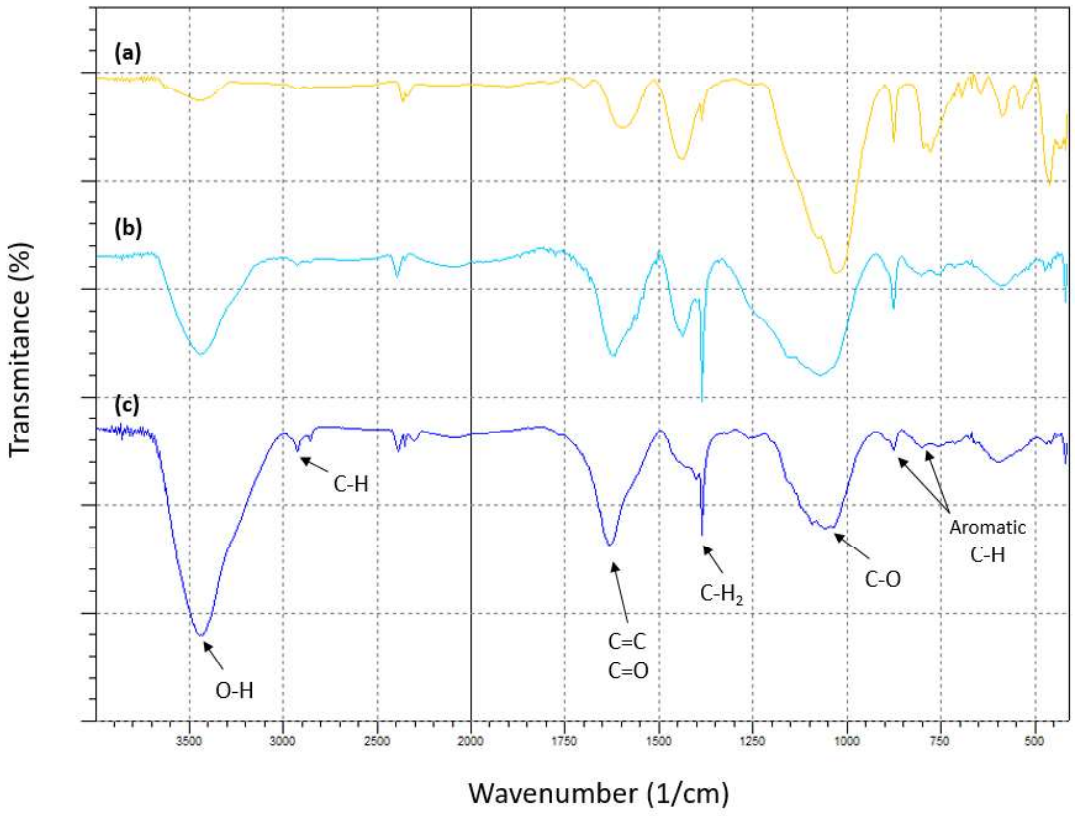

258

259 ***Figure 1***. FTIR spectra of (a) BC and ba-BC after (b) 9 and (c) 30 days of co-composting.

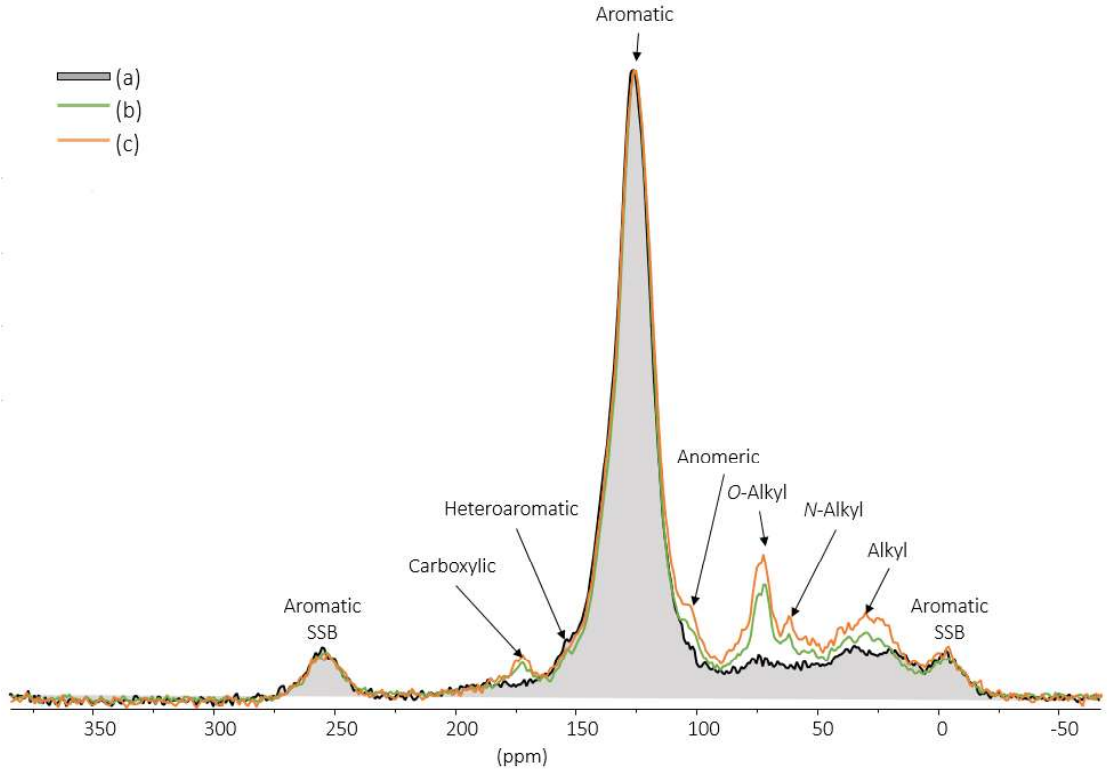

260

Figure 2. ^{13}C-NMR spectra of (a) BC and ba-BC after (b) 9 and (c) 30 days co-composting. Spectral regions in which carbon atoms resonate were assigned according to Knicker (2011) [52]. Note that two peaks correspond to the spinning sidebands (SSB) of the aromatic one.

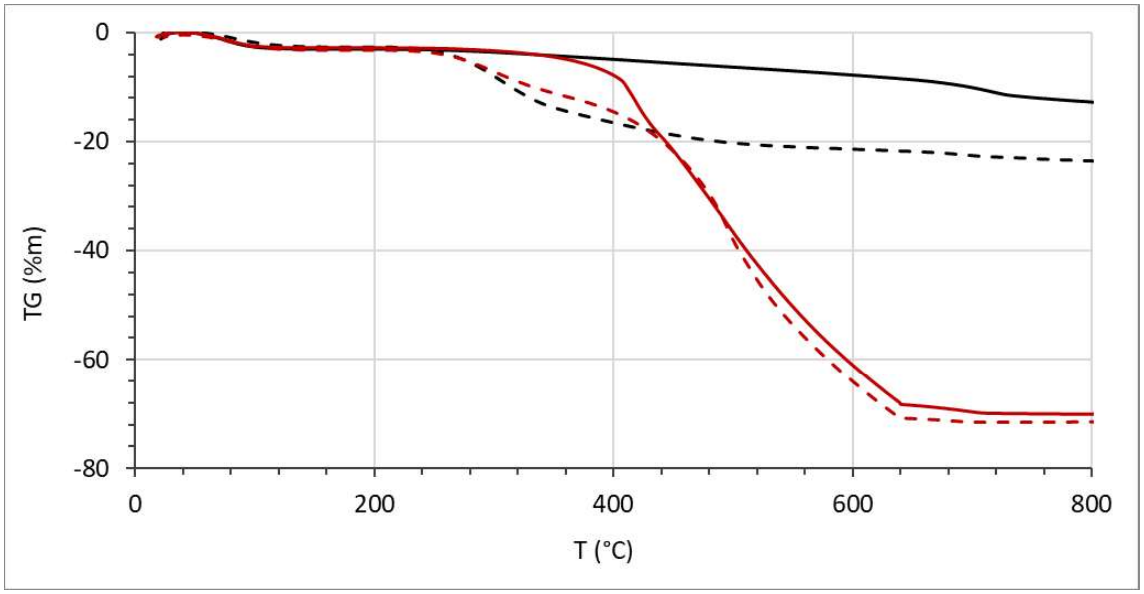

Figure 3. Thermogravimetric analysis of BC (solid line) and ba-BC (dashed line) in He (black) and in air (red).

BET surface area of biochar remains almost unaltered after the biochemical aging (obtained from P/P_0 region between 0.05-0.30 of the adsorption isotherms, type I) but it increases by an order of magnitude when physical aging is applied *(Table 1 and Figure 4a)*. Consistently with these results, micropore volume and pore area are also an order of magnitude higher in physically aged samples which shows, in addition, a deep reduction in particle size.

Results of Hg intrusion porosimetry *(Table 1 and Figure 4b)* provide information about macroporosity in the studied samples. Biochar before and after biochemical aging exhibits two different macroporous characterized by approximately 1 and 10 µm pore diameter, respectively. After physical aging, the porosity at 10 µm disappears, leading to a sharp porosity distribution at ~1 µm. The total Hg intrusion volume and total area is higher in physically unaged samples, because of the disappearance of the porosity at 10 µm after samples were ball-milled. To avoid ambiguous and field-specific expressions in terms of pore size ranges,

such as macro-, meso- and microporosity, the authors defined the ranges meaningful for this study as small, medium and large pore-size as as defined in *Table 2.*

Table 1. Particle size distribution, N_2 adsorption and Hg intrusion porosimetry results of unaged (BC), physically aged (pa-BC), biochemically aged (ba-BC) and physically and biochemically aged biochar (pba-BC).

	Particle size distribution	**N_2 adsorption porosimetry**			**Hg intrusion porosimetry**	
	Mean (µm)	**BET surface area ($m^2 g^{-1}$)**	**Micropore volume ($cm^3 g^{-1}$)**	**Pore area ($m^2 g^{-1}$)**	**Total intrusion volume ($mL g^{-1}$)**	**Total area ($m^2 g^{-1}$)**
BC	2×10^3	22.15	0.015	4.36	1.41	14.76
ba-BC	2×10^3	20.50	0.011	2.91	1.35	13.39
pa-BC	7 / 75 *(bimodal distribution)	176.01	0.121	22.48	0.85	7.55
pba-BC	9	311.19	0.201	20.91	1.03	7.96

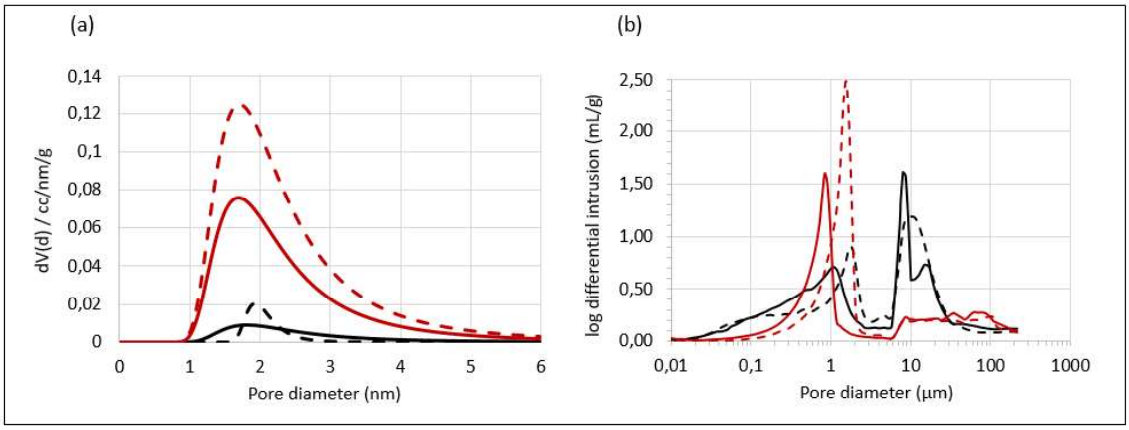

Figure 4. (a) BJH porosimetric analysis of N_2 adsorption isotherms and (b) Hg intrusion porosimetry analysis of BC (black solid line) and ba-BC (black dashed line), pa-BC (red solid line) and pba-BC (red dashed line).

Table 2. Definition of porosity ranges

Porosity range	**Pore size**
Small-size pores	1 – 5 nm
Medium-size pores	5 – 500 nm
Large-size pores	0.5 - 50 µm

Biochar interactions with water

^{1}H NMR relaxometry measurements were carried out to evaluate biochar-water interactions using the T_1 and T_2 NMR observables, as it was previously described. Results were collected from samples with adsorbed water from controlled RH atmospheres and from samples in liquid water.

In samples with adsorbed water, the proton intensity of the peaks of T_2 NMR relaxation distribution increases as expected with relative humidity, as there is more water adsorbed in the sample *(Figure 5).* At this point it is important to remark that for all dry samples, in absence of adsorbed water (0% RH), proton signal was not detectable, suggesting that structural protons of biochar before and after aging are not visible with the parameters used in this work. To verify this statement in presence of water (i.e., the actual conditions for the set of studied samples) and check if water interactions could augment the mobility of structural protons (increasing their T_2 NMR values and making them visible in the NMR experiments), dry samples were wetted with D_2O to establish water-biochar interaction without providing additional hydrogen atoms from water. No changes in NMR signal was either appreciated, demonstrating that structural protons have no effects on the reported NMR results. The small signal measured *(Supplementary Information, Figure SI-2)* is attributed to a minor replacement of deuterium ions by hydrogen ions from atmospheric humidity.

The maxima of the broad and asymmetrical distribution of T_2 NMR relaxation times in presence of adsorbed water in biochar before and after biochemical aging (BC and ba-BC) appear at 3-4 ms whereas it is slightly shifted to lower times (around 1 ms) in physically aged samples (pa-BC and pba-BC). These results allow us characterize the T_2 NMR relaxation times of water interacting with biochar at RH < 100 %.

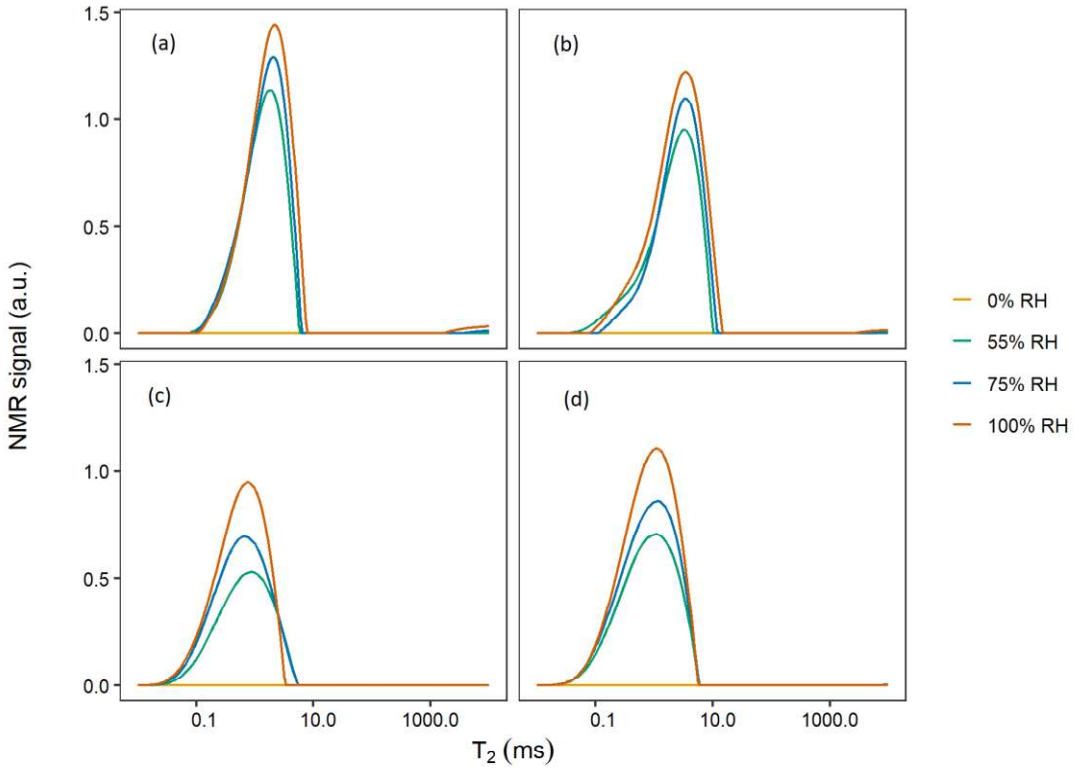

315

316 ***Figure 5***. ^{1}H NMR relaxometry of (a) BC, (b) ba-BC, (c) pa-BC and (d) pba-BC at 0, 55, 75 and 100% of relative

317 humidity.

318

319 T_2 NMR relaxation time distributions of samples obtained with biochar and liquid water (using

320 the same 1:4 mass ratio for all samples) are shown in *Figure 6.* After 30 minutes, the added

321 water is able to distribute similarly in BC and ba-BC, whereas the effect of physical aging is

322 evident in pa-BC and pba-BC, as the amount of water with short T_2 values (small pores) has

323 greatly increased. In BC and ba-BC water protons show a complex behaviour, being possible to

324 differentiate four different T_2 values with maxima at approximately 5, 50, 500 and 2000 ms.

325 The main signal at 2000 ms is attributed to the relaxation time of water outside the sample

326 [53], representing more than 50% of the total intensity at t=30 min. After 7 and 30 days this

327 signal at 2000 ms disappears and its intensity is redistributed to the intermediate water signals

328 characterized by a relaxation time at 500 ms for BC and at 200 ms for ba-BC, becoming the

329 main signal for water in these samples. The faster T_2 relaxation times remain at 5-10 ms and

330 around 50 ms and their intensity does not increase with time.

On the other hand, physically aged samples exhibit a small (~ 10% for pa-BC) or absent (pba-BC) contribution of water outside the sample (characterized by a relaxation time around 2000 ms) after a short treatment time (e.g., t=30 min), indicating that most of the water interacts almost immediately with biochar. This rapid interaction is observed as the NMR value of water with the long T_2 decrease during the first 30 minutes and then stay constant over 30 days. Opposite to the behaviour described for BC and ba-BC, after 30 minutes of treatment the higher fraction of water signal relaxes at 10 ms and its intensity remains almost constant for physically aged samples. In addition, there is a decrease of T_2 NMR values for this peak (this is clearer for pba-BC but the same tendency is observed for pa-BC). Compared to physically unaged samples, another signal was found at 100-200 ms which follows different patterns for pa-BC and pba-BC. A low intensity and constant signal with time for pa-BC and a sharp increase with time for pba-BC.

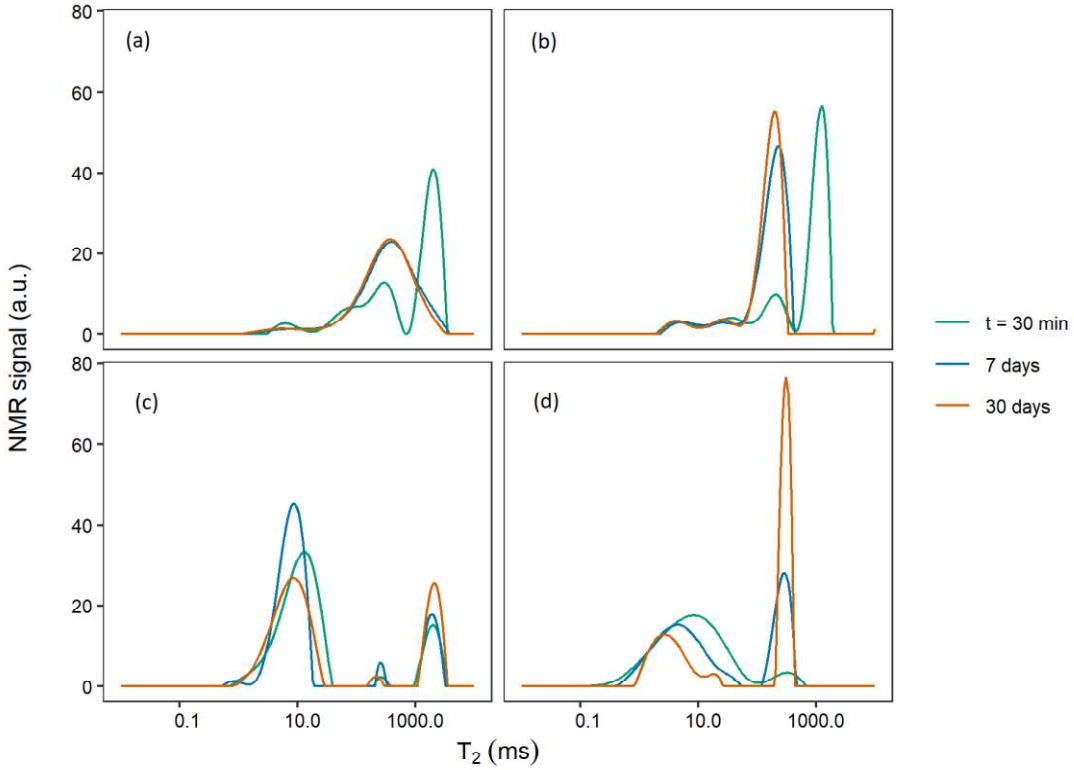

Figure 6. ^{1}H NMR relaxometry of (a) BC, (b) ba-BC, (c) pa-BC and (d) pba-BC with liquid water after 30 minutes, 7 days, and 30 days.

In T_1-T_2 ^{1}H NMR relaxometry spectra of physically unaged samples *(Figures 7a and 7b),* most water signal is placed close to the T_1=T_2 line, indicating different degrees of confinement caused by the size of the pores *(Table 2)* [54]. The highest intensity signal, in the 100-1000 ms range and falling straight in the T_1=T_2 line, corresponds to water in larger size pores, while the signal exhibiting lower T_1-T_2 ratios (10-100 and 1-10 ms) is placed slightly below the T_1=T_2 line indicating lower water dynamics. Three regions with different T_1-T_2 ratios were observed in BC (1.68, 2.52 and 4.50) and ba-BC (1.30, 2.12 and 3.78), while two regions were differentiated in pa-BC (3.00 and 4.25) and pba-BC (1.12 and 8.50). For physically aged biochar samples *(Figures 7c and 7d*), the region with high T_1 and T_2 values (100-1000 ms), which is close to the T_1=T_2 line, shows a higher T_1-T_2 ratio for *Figure 7c* and the region with low relaxation time values (1-50 ms) shows a higher T_1-T_2 ratio (*Figure 7d*) in comparison to the other 3 spectra.

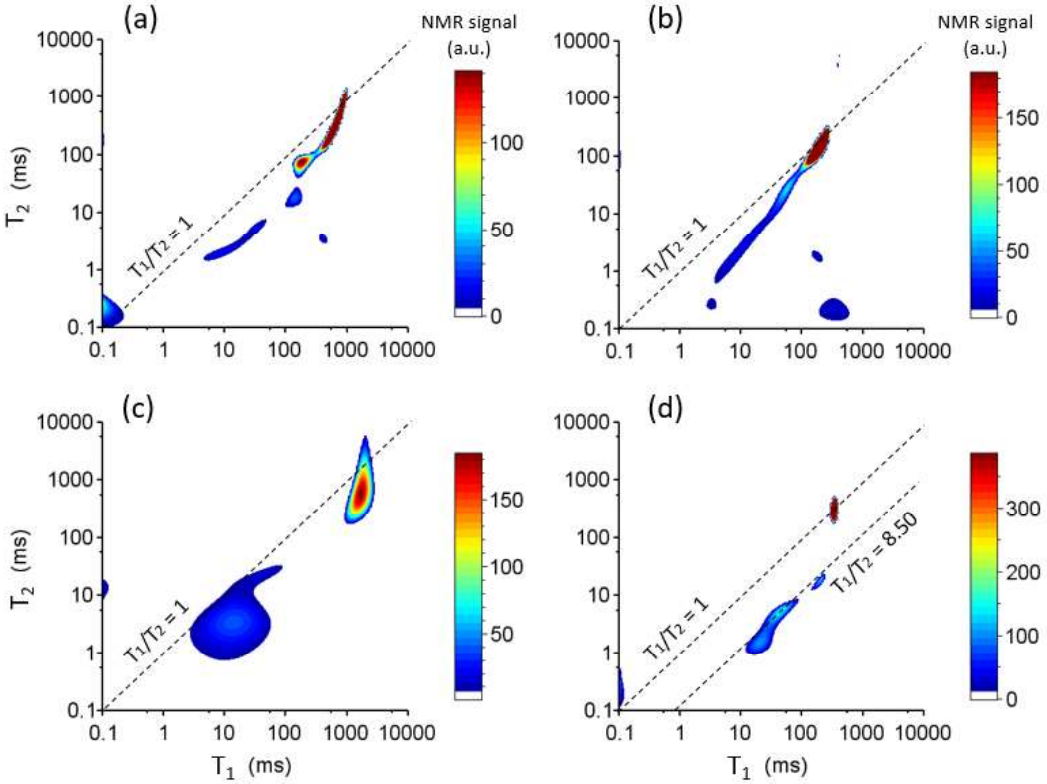

Figure 7. T_1-T_2 ^{1}H NMR relaxometry correlation spectra of (a) BC, (b) ba-BC, (c) pa-BC and (d) pba-BC with liquid water.

Discussion

Chemical and physical alteration of biochar during aging

The properties of unaged biochar vary depending on the nature of the feedstock and pyrolysis conditions of the process, in terms of chemical composition and stability, reactivity and porosity [20]. Besides, it has been described that biochar undergoes several physicochemical changes in contact with soil and during co-composting processes [11,54-56]. This aging process could be related to biotic and/or abiotic processes. Abiotic aging could be mainly attributed to the physical disruption of biochar coarse particles, exposing internal surfaces of the biochar skeleton and thus changing its porosity and reactivity. Biotic aging is mediated by microbial communities which could directly feed on biochar reactive surfaces edges [10] or use biochar pore space as habitat [57].

In this study, two different factors of biochar aging were studied to understand the changes undergoing in the material. On one hand, we considered the effect of 30-day co-composting process of prune and coffee on wood biochar (biochemical or biotic aging) and, on the other hand, we evaluated the physical disruption of the biochar particle (physical or abiotic aging) and the combined effect of both processes.

According to the data obtained by FTIR analysis, pristine biochar spectrum exhibits bands corresponding to stable carbon forms, characteristic of pyrolyzed organic matter with a clear aromatic ring input and a series of bands in the 650-1800 cm^{-1} range that is attributed to non-pyrolyzed lignocellulosic remains [58]. The presence of oxygenated functionalities is more evident after 9 and 30-days co-composting process, where the spectrum exhibits a higher signal corresponding to functional groups, indicating the presence of fresh organic matter or minerals obtained in contact with compost and microbial activity [59]. This is consistent with the bands attributed to aliphatic C-H stretching, suggesting the presence of plant lipids (i.e., suberines, cutines, surface wax) or microbial lipids (i.e., membrane phospholipids) which

388 appear after co-composting. These results are also in agreement with the data obtained by ^{13}C
389 solid state NMR, where an increase in the signals of *O*-alkyl and alkyl groups is appreciated.
390 The continuous increase of signal during co-composting on the areas of *O*-alkyl and alkyl
391 groups (in comparison to aromatic signal) indicates a process of surface functionalisation or
392 strong adsorption of labile organic matter on biochar, rather than a physical mixture of biochar
393 and compost. However, direct functionalization of the aromatic rings cannot be assessed due
394 to the overlapping of the heteroaromatic peak with the large aromatic one. The combination
395 of both techniques shows that biochar undergoes surface functionalisation with acidic groups
396 in non-aromatic chains, coming from the interaction with compost and by microbial activity.
397 These results could also be explained by the presence of fresh organic matter coating on the
398 surface and within pores of biochar created during the co-composting process, as reported by
399 several authors [9,11,14]. This biochemical aging of biochar during co-composting is also
400 appreciated in thermogravimetric analysis. Mass loss difference in the 250-350 °C range
401 between both materials (in He and air atmospheres) indicates the presence of labile organic
402 compounds coming from functional groups generated in the co-composting process by the
403 interaction of biochar and compost, or from the decomposition of biochar by microbial
404 activity. Both samples exhibit rather high final residue of approximately 30% m/m
405 corresponding to ash and remnants of high recalcitrance.
406 Aging process also affects the physical properties of biochar, as seen in the results by
407 porosimetric analysis by Hg intrusion and N_2 adsorption. The porosity in the large pore-size
408 range (>0.5 µm) measured by Hg intrusion porosimetry described how physically unaged
409 samples exhibit two well defined porosity regimes at 1 and 10 µm pore diameter. After ball-
410 milling (simulating physical aging) the porosity at 10 µm is lost, leading to a single well-defined
411 porosity with a mean value of pore size distribution 1 µm. No reduction of pore size diameter
412 was appreciated after biochemical aging, which indicates that if a coating layer is formed on
413 the small size pore walls, it has no effect in the pore diameter at this scale. Regarding N_2

adsorption measurements, it is worth noting that all measured samples exhibit hysteresis between N_2 adsorption and desorption isotherms in all the range of P/P_0 values. This is not a type IV isotherm hysteresis caused by the capillarity in mesopores as it appears in the whole P/P_0 range. This hysteresis is attributed to the entrapment of N_2 gas in the pores which is an effect sometimes appreciated in carbon materials [60] and biochars [61]. In terms of BET surface area results, there is an expected difference of an order of magnitude for physically aged samples because of the reduction of particle size after the grinding process. Milled samples (both after and before biochemical aging) exhibit porosity in the small size pore range (1-5 nm), characteristic of this kind of carbon materials. In this sense, bulk samples are characterized by a particle size distribution at 2 mm diameter size, whereas ground samples exhibit a bimodal distribution with maxima at 7 and 75 µm after physically aging and a single mean value of 9 µm for the biochemically aged.

Water distribution and interactions with biochar as affected by aging

^{1}H NMR relaxometry measurements were carried out to obtain the T_2 NMR relaxation distributions to estimate the distribution of water on different biochar porosities for unaged and aged samples in contact with adsorbed and liquid water. This also allowed understanding the effect of biochemical aging during co-composting process, which are reported to be comparable to aging within the soil matrix [4]. Similarly, ball-milled samples were analysed and compared to bulk samples to address the effect of physical aging, weathering, or physical disruption that biochar undergoes with time after its application to soils.

Regarding the obtained results, it is important to note that there is not observable NMR signal from protons coming from dry samples, demonstrating that structural hydrogen atoms from biochar after and before aging have faster relaxation times than the spectrometer dead time. To verify if structural hydrogen atoms could increase their relaxation times in presence of water and, thus, contribute to the total measured intensities, dry samples were mixed with

440 deuterated water (D_2O) producing water-biochar interactions but without providing protons
441 from water. Results exhibited no increase in the signal *(Figure SI-2)*, indicating that structural
442 hydrogen atoms of biochar do not provide relevant proton NMR signal for our experimental
443 condition and, thus, all incoming NMR signals for these samples will correspond only to
444 adsorbed water.
445 The relatively short transverse relaxation times obtained for biochar at RH > 50% is assigned to
446 water adsorbed to the surface of the particle (and pores), probably attached to remaining
447 functional groups and structural defects, describing strong interactions that do not allow fast
448 proton dynamics. However, as the amount of adsorbed water is relatively high *(Water*
449 *Retention Capacity (WRC) data showed in supplementary information, Table SI-1)* and similar
450 to what we can observe in wood samples (where the amount of functional groups is more
451 important) [35], thus other mechanisms could contribute to adsorption of water in biochar.
452 Relaxation time is shorter for ball-milled (simulating physical aging) samples (1 ms) than for
453 bulk samples (3-4 ms) probably because of a higher surface interaction due to the increase on
454 surface area or to the accessibility of water to smaller and inner pores after ball-milling.
455 T_2 NMR relaxation time results of liquid water in contact with physically unaged biochar before
456 and after biochemical aging (BC and ba-BC) *(Figure 6a and 6b)* indicate that after 30 minutes of
457 contact between water and the biochar, the liquid distributes similarly in both materials. In
458 these samples water shows a complex transverse relaxation behaviour with at least four quite
459 different relaxation times measured at around 2000, 500, 50 and 5 ms, respectively. The signal
460 at the largest T_2 time, e.g. 2000 ms, is attributed to the relaxation time of free water outside
461 the sample [62], indicating that after 30 minutes, more than 50% of the added water remains
462 without any interaction with the biochar. Results after 7 and 30 days show the progressive
463 disappearance of the signal at 2000 ms and an increment in the intensity at intermediate
464 relaxation times (500 ms for BC and 200 ms for ba-BC), indicating that water permeates into
465 the large pore size system with time. The intensities of the shorter T_2 NMR peaks (at 50 and 5

466 ms) remain constant with time, indicating that the small (and accessible) porosity regimes are
467 filled with a water fraction at the first stages of imbibition, remaining unaltered with the time.
468 It demonstrates that the number of small and accessible pores does not increase with the
469 exposure time. Each of these relaxation times correspond to water confined in a certain
470 porosity regime, which has also been defined as transmission like (>50 µm), storage-like (50-5
471 µm) and residual-like (<5 µm) pores in soil samples [63] and used as well for biochar studies
472 [18]. Following this classification, the intermediate T_2 signal measured at steady state could be
473 attributed to water in transmission and storage like pores where a relatively high mobility of
474 water is allowed. The shorter T_2 NMR values could be attributed to storage and residual-like
475 pores where water loses mobility because of a higher degree of confinement and, arguably,
476 due to the interactions with the surface of the pore walls. It is worth noting that the shortest
477 T_2 values are rather similar to that measured for adsorbed water (1-3 ms), which may be
478 understood as a shared contribution of small pore size and surface adsorption, which would
479 decrease the overall mobility of water molecules, provoking a faster transverse NMR
480 relaxation of water molecules (lower T_2 values) because of increasing dipolar interactions [17].
481 Water added to physically aged samples *(Figures 6c and 6d)* exhibit significantly shorter T_2
482 relaxation times after 30 minutes of treatment when they are compared with bulk samples. It
483 indicates that interaction of water with the biochar is strongly affected by the variation in the
484 particle size and pore structure caused by the ball-milling process. On the one hand, the
485 reduction in the particle size promotes a faster interaction of the added water with biochar,
486 showing a deep decrease or even the disappearance of free water (characterized by a
487 relaxation time T_2 around 2000 ms) in pba-BC after 30minutes. On the other hand, the water
488 fraction with restricted mobility, i.e., those characterized by a shorter relaxation time [62],
489 increases after ball-milling. This behaviour could be explained by the combination of different
490 factors, such as the increase in surface area and an improved access to the small size pores
491 volume as well as the reduction in the inter-aggregate space between biochar particles, that

492 increases the overall fraction of interacting water with shorter relaxation times. Nevertheless,
493 the interaction of water at the surface, in the small size pores or at the inter-aggregate space
494 appears to be different, which can be the cause of the observed differences on water mobility
495 and hence, in the corresponding NMR relaxation time [35]. In pa-BC, however, there is a T_2
496 signal at 2000 ms which is attributed to an excess of water that remains outside the sample
497 after all the inter-aggregate spaces of the system were saturated, which could increase
498 because of particle sedimentation over time.
499 T_1-T_2 spectra at steady state for physically unaged samples (BC and ba-BC) show three different
500 regions. The strongest signal, at long T_1 and T_2 values, corresponds to free water with high
501 mobility which falls straight in the T_1=T_2 line, presumably water that permeated in the large
502 pore size system of the material. The two regions at lower T_1-T_2 ratios would correspond to
503 water in a higher surface-to-volume ratio system, this is, smaller porosity regime. As they
504 appear slightly below the T_1=T_2 line, lower dynamics (molecular tumbling) could be assumed by
505 a certain degree of adsorption or interactions with the material reactive surfaces. In T_1-T_2
506 spectra at steady state of ball-milled samples (pa-BC and pba-BC) the high-mobility free water,
507 with the most intense peak in the 100-1000 ms range it is clearly differentiated from water
508 placed in the smaller porosity regime [50]. After biochemical aging, T_1-T_2 ratios for the three
509 different regions are similar to that of BC sample, indicating the higher degree of chemical
510 functionalisation originated from the composting process is not increasing water adsorption. In
511 addition, after physical aging we do not see an increase of T_1-T_2 ratio for the water in the
512 smaller porosity (which is likely to be the water that interacts strongly with biochar) but we see
513 an increase of the T_1-T_2 ratio for the water in the larger porosity. However, it seems that this
514 effect should be important as for the pba-BC sample we can see and important increase on the
515 T_1-T_2 for the water in smaller porosities (from about 4 to 8).
516 The capacity of biochar to retain water in their structure is crucial to understand the mobility
517 and availability of nutrients for plants. The water placed in the inter-aggregate space and in

large size pores (*i.e.* transmission-like) can move and permeate easily between biochar and soil being easily available for the roots of the plant. As a counterpart, water in this state can also be more easily lost by evaporation or diffusion. Actually, we can see that some of this water transfer from the inter-aggregate state to a more mobile state over the 30 days but the amount is relatively low, showing the capability of aged biochar to keep water for long periods of time. In addition, water in medium size pores (i.e. storage-like) exhibit stronger interactions and is longer retained, providing an attractive water/nutrient "pool" for plants and microorganisms. Finally, water in small size pores (i.e. residual-like) appears to be strongly bonded to the material and would require certain negative pressure by root suction to be available [63]. To allow the assignment of each of the T_2 signals to a specific porosity regime further studies are needed with deep analysis in ^{1}H NMR relaxometry and porosimetry techniques.

Conclusions

This study indicates that a surface modification in chemical composition of biochar takes place during co-composting process, with an enrichment of oxygen functionalities. The mobility and plant availability of soil cations such as nutrients and contaminants will be dependent of water mobility throughout the soil matrix and its and its porosity, making biochar/water interactions a key issue in the understanding of the role of this material as soil amendment. ^{1}H NMR relaxometry results indicate that water interacts in a more intimate manner with biochar, exhibiting shorter T_2 NMR relaxation times and slightly higher T_1-T_2 ratios, after the biochemical aging process, probably due to a higher wettability and stronger interactions with the functionalised surface. Particle size reduction has a clear effect in the interaction with water, making stronger and faster interactions when particle size is reduced as proved by ^{1}H NMR relaxometry. Water placed in the inter-aggregate porosity is the main contributor to lower T_2 times. Physical and biochemical aging of biochar is therefore critical to understand the

544 enhancement on the agronomic performance of biochar with time when used as amendment
545 in soils, not only because of the enrichment in nutrients, but also because of water dynamics
546 and retention capacity in biochar particles.
547
548 **Acknowledgements**
549 This study was financially supported by the Comunidad de Madrid and the Spanish National
550 Research Council (CSIC) research grant Atracción de Talento [grant number
551 2019T1/AMB14503]. The authors acknowledge the funding received from the Spanish National
552 Research Council and the French National Centre for Scientific Research through the
553 cooperation project PICS [grant number 018FR0044] and IEA (ex-PICS) grant number 203026,
554 respectively. This work was also partially funded by the Spanish Ministerio de Ciencia e
555 Innovación (PTA2018-015282-I and PID2020-119047RB-I00) and Comunidad de Madrid (PEJ-
556 2018-TL/IND-11075). The authors want to thank the analytical services for the ^{1}H relaxometry
557 NMR at ICTP-CSIC, for the solid state ^{13}C NMR at IRNAS-CSIC and for FT-IR, TGA and
558 porosimetry analyses at ICA-CSIC. Technical support provided by Mr. Héctor Fritis, Ms. Cristina
559 Gómez Ruano, Mr. David Mabilais, Mr. Fernando Martín Salamanca and Dr. Rebeca Herrero is
560 gratefully acknowledged.
561
562 **Credit Author Statement**
563 Asier Goñi-Urtiaga: Investigation, Methodology, Writing-Original Draft. Denis Courtier-Murias:
564 Conceptualization, Data curation, Methodology, Writing-review & editing, Validation.
565 Giuseppe Picca: Investigation. Juan López-Valentín: Methodology, Reviewing. César Plaza:
566 Reviewing, Validation. Marco Panettieri: Supervision, Conceptualization, Funding acquisition,
567 Writing-review & editing, Validation.
568
569 **References**

[1] S. Joseph, A.L. Cowie, L. Van Zwieten, N. Bolan, A. Budai, W. Buss, M.L. Cayuela, E.R. Graber, J.A. Ippolito, Y, Kuzyakov, Y. Luo, Y. Sik Ok, K.N. Palansooriya, J. Shepherd, S. Stephens, Z.H. Weng and J. Lehmann. *How biochar works, and when it doesn't: A review of mechanisms controlling soil and plant responses to biochar*. GCB Bioenergy, (00), pp. 1–34 (2021).

[2] S. Schimmelpfennig, B. Glaser. *One Step Forward toward Characterization: Some Important Material Properties to Distinguish Biochars*. Journal of Environmental Quality, 41, pp. 1001-1013 (2012).

[3] J. Lehman. *A hand full of carbon.* Nature, 447, pp. 143–144 (2007).

[4] L. Wang, D. O´Connor, J. Rinklebe, Y. Sik Ok, D. C.W. Tsang and D. Hou. *Biochar Aging: Mechanisms, Physicochemical Changes, Assessment, And Implications for Field Applications.* Environmental Science & Technology. 54, 23, pp. 14797–14814 (2020).

[5] Y. Kuzyakov, I. Bogomolova, B. Glaser. *Biochar stability in soil: Decomposition during eight years and transformation as assessed by compound-specific ^{14}C analysis*. Soil Biology and Biochemistry, 70, pp. 229- 236 (2014).

[6] A. Gross, T. Bromm, B. Glaser. *Soil Organic Carbon Sequestration after Biochar Application: A Global Meta-Analysis*. Agronomy, 11, pp. 2474 (2021).

[7] G. Agegnehu, A.K. Srivastava and M.I. Bird. *The role of biochar and biochar-compost in improving soil quality and crop performance: A review*. Applied Soil Ecology, 119, pp. 156–170 (2017).

[8] G. Fellet, P. Conte, V. Bortolotti, F. Zama, G. Landi, DF. Chillura Martino, V. Ferro, L. Marchiol, P. Lo Meo. *Changes in physical-chemical biochar properties following addition to soil*. Agriculture, 12 p. 320 (2022).

[9] C. I. Kamman, H.P. Schmidt, N. Messerschmidt, S. Linsel, D. Steffens, C. Müller, H. W. Koyro, P. Conte and S. Joseph. *Plant growth improvement mediated by nitrate capture in co-composted biochar*. Scientific Reports, 5, nº 11080 (2015).

[10] K. Wiedner, D. Fischer, S. Walther, I. Criscuoli, F. Favilli, O. Nelle and B. Glaser. *Acceleration of Biochar Surface Oxidation during Composting?* Journal of Agricultural and Food Chemistry, 63, pp. 3830-3837 (2015).

[11] S. Joseph, C. I. Kammann, J. G. Shepherd, P. Conte, H. Schmidt, N. Hagemann, A. M. Rich, C. E. Marjo, J. Allen, P. Munroe. *Microstructural and associated chemical changes during the composting of a high temperature biochar: mechanisms for nitrate, phosphate and other nutrient retention and release*. Science of The Total Environment, 618, pp. 1210-1223 (2018).

[12] M. Nocentini, M. Panettieri, J. M. García de Castro Barragán, G. Mastrolonardo, H. Knicker. *Recycling pyrolyzed organic waste from plant nurseries, rice production and shrimp industry as peat substitute in potting substrates.* Journal of Environmental Management, 277, p. 111436 (2021).

[13] D. Fischer, B. Glaser. *Synergisms between Compost and Biochar for Sustainable Soil Amelioration. In: Management of Organic Waste*. InTech, pp 167-198 (2012).

[14] N. Hagemann, S. Joseph, H. Schmidt, C. Kammann, J. Harter, T. Borch, R. B. Young, K. Varga, S. Taherymoosavi, K. Elliott, A. McKenna, M. Albu, C. Mayrhofer, M. Obst, P. Conte, A. Dieguez-Alonso, S. Orsetti, E. Subdiaga, S. Behrens and A. Kappler. *Organic coating on biochar explains its nutrient retention and stimulation of soil fertility.* Nature Communications, 8, p. 1089 (2017).

615 [15] G. Baiamonte, C. De Pasquale, V. Marsala, G. Cimò, G. Alonzo, G. Crescimanno, P. Conte.
616 *Structure alteration of a sandy-clay soil by biochar amendments*. Journal of Soils and
617 Sediments (2014).

618 [16] P. Conte, U. M. Hanke, V. Marsala, G. Cimò, G. Alonzo, B. Glaser. *Mechanisms of water*
619 *interaction with pore systems of hydrochar and pyrochar from poplar forestry waste*.
620 Journal of Agricultural and Food Chemistry. 62, pp. 4917–4923 (2014).

621 [17] P. Conte, V. Marsala, C. De Pasquale, S. Bubici, M. Valagussa, A. Pozzi,G. Alonzo. *Nature of*
622 *water-biochar interface interactions*. GCB Bioenergy, 5, pp. 116–121 (2013).

623 [18] P. Conte and N. Nestle*. Water dynamics in different biochar fractions.* Magnetic
624 Resonance in Chemistry, (2015).

625 [19] E. M. C. C. Batista, J. Shultz, T. T. S. Matos, M. R. Fornari, T. M. Ferreira, B. Szpoganicz, R.
626 A. de Freitas and A. S. Mangrich. *Effect of surface and porosity of biochar on water holding*
627 *capacity aiming indirectly at preservation of the Amazon biome*. Scientific Reports, 8,
628 nº 10677 (2018).

629 [20] H. Huang, N. Gangadhara Reddy, X. Huang, P. Chen, P. Wang, Y. Zhang, Y. Huang, P.
630 Lin and A. Garg. *Effects of pyrolysis temperature, feedstock type and compaction on water*
631 *retention of biochar amended soil.* Scientific Reports, 11, nº 7419 (2021).

632 [21] P. Faure, S. Caré, C. Po, S. Rodts. *An MRI-SPI and NMR relaxation study of drying-hydration*
633 *coupling effect on microstructure of cement-based materials at early age*. Magnetic Resonance
634 Imaging, 23, pp. 311–314.33 (2005).

635 [22] P. Faure, U. Peter, D. Lesueur, P. Coussot. *Water transfers within Hemp Lime Concrete*
636 *followed by NMR.* Cement and Concrete Research, 42, pp.1468–1474 (2012).

637 [23] P. Faure, S. Rodts. *Proton NMR relaxation as a probe for setting cement pastes*. Magnetic
638 Resonance Imaging, 26, pp. 1183–1196 (2008).

[24] N. Labbé, B. De Jéso, J.C. Lartigue, G. Daudé, M. Pétraud, M. Ratier. *Moisture content and extractive materials in Maritime Pine wood by low field ^{1}H NMR.* Holzforschung, 56, pp. 25–31 (2002).

[25] H. Penvern, M. Zhou, B. Maillet, D. Courtier-Murias, M. Scheel, J. Perrin, T. Weitkamp, S. Bardet, S. Caré and P. Coussot. *How Bound Water Regulates Wood Drying*. Physical Review Applied, 14 (2020).

[26] M. Urbańczyk, Y. Kharbanda, O. Mankinen, and V-V. Telkki. *Accelerating Restricted Diffusion NMR Studies with Time-Resolved and Ultrafast Methods*. Analytical Chemistry, 92, 14, pp. 9948–9955 (2020).

[27] A. Sharp, M. Riggin, R. Kaiser. *Determination of moisture content of wood by pulsed nuclear magnetic resonance*. Wood Fiber Science, 10, pp. 74–81 (1978).

[28] R. S. Menon, A. L. MaCkay, J. R. T. Hailey, M. Bloom, A. E. Burgess, J. S. Swanson. *An NMR determination of the physiological water distribution in wood during drying*. Journal of Applied Polymer Science, 33, pp. 1141–1155 (1987).

[29] C.D. Araujo, A.L. MacKay, J.R.T. Hailey, K.P. Whittall. *Proton magnetic resonance techniques for characterization of water in wood: application to white spruce*. Wood Science Technology, 26, pp. 101–113 (1992).

[30] N. Labbé, B. De Jéso, J.C. Lartigue, G. Daudé, M. Pétraud, M. Ratier. *Moisture content and extractive materials in Maritime Pine wood by low field ^{1}H NMR.* Holzforschung, 56, pp.25–31 (2002).

[31] G. Almeida, S. Gagné, R.E. Hernandez. *A NMR study of water distribution in hardwoods at several equilibrium moisture contents*. Wood Science Technology, 41, pp.293–307 (2007).

[32] V.V. Telkki, M. Yliniemi, J. Jokisaari. *Moisture in softwoods: fiber saturation point, hydroxyl site content, and the amount of micropores as determined from NMR relaxation time distributions.* Holzforschung, 67(3), pp.291-300 (2013).

[33] C.D. Araujo, S. Avramidis, A.L. MacKay. *Behaviour of solid wood and bound water as a function of moisture content: a proton magnetic resonance study*. Holzforschung, 48, pp. 69–74 (1994).

[34] J. Cox, P. J. McDonald and B. A. Gardiner. *A study of water exchange in wood by means of 2D NMR relaxation correlation and Exchange.* Holzforschung, 64, pp. 259–266 (2010).

[35] M. Bonnet, D. Courtier-Murias, P. Faure, S. Rodts and S. Care. *NMR determination of sorption isotherms in earlywood and latewood of Douglas fir. Identification of bound water components related to their local environment*. Holzforschung, 71 (6), pp. 481-490 (2017).

[36] T. Jeoh, N. Karuna, N.D. Weiss and L.G. Thygesen. *Two-Dimensional ^{1}H-Nuclear Magnetic Resonance Relaxometry for Understanding Biomass Recalcitrance*. ACS Sustainable Chemistry & Engineering, 5, 10 pp. 8785–8795 (2017).

[37] Z. Liu, N. Qi, Y. Luan and X. Sun. *Thermogravimetry-Infrared Spectroscopy Analysis of the Pyrolysis of Willow Leaves, Stems and branches.* Advances in Material Science and Engineering, nº 303212 (2015).

[38] T. Carballo, M. V. Gil, X. Gómez and F. González-Andrés. *Characterization of different compost extracts using Fourier-transform infrared spectroscopy (FTIR) and thermal analysis.* Biodegradation, 19 (6), pp. 815-30 (2008).

[39] K. Sing. *The use of nitrogen adsorption for the characterisation of porous Materials.* Colloids and Surfaces; A: Physicochemical and Engineering Aspects,187–188, pp. 3–9 (2001).

[40] H. Giesche. *Mercury Porosimetry: A General (Practical) Overview*. Particle & Particle System Characterization ,23, pp. 9–19 (2006).

[41] D. Courtier-Murias, H. Farooq, J.G. Longstaffe, B.P. Kelleher, K.M. Hart, M.J. Simpson and A.J. Simpson. *Cross polarization-single pulse/magic angle spinning (CPSP/MAS): A robust technique for routine soil analysis by solid-state NMR*. Geoderma, 226–227, pp. 405-414 (2014).

[42] H. Knicker, M. Velasco-Molina and M. Nicker. *2D Solid-State HETCOR ^{1}H-^{13}C NMR Experiments with Variable Cross Polarization Times as a Tool for a Better Understanding of the Chemistry of Cellulose-Based Pyrochars—A Tutorial***.** Applied Science, 11(18), 8569 (2021).

[43] H. Knicker. *Soil organic N - An under-rated player for C sequestration in soils?* Soil Biology and Biochemistry, 43 (6), pp. 1118-1129 (2011).

[44] H. D. Ludemann and H. Nimz. *Carbon-13 nuclear magnetic resonance spectra of lignins*. Biochemical and Biophysical Research Communications, 52 (4), pp. 1162-1169 (1973).

[45] H. Y. Carr and E. M. Purcell. *Effects of Diffusion on Free Precession in Nuclear Magnetic Resonance Experiments.* Physical Review Journal Archive, 94, p. 630 (1954).

[46] S. Meiboom and D. Gill. *Modified Spin-Echo Method for Measuring Nuclear Relaxation Times*. Review of Scientific Instruments, 29 (8), pp. 688-691 (1958).

[47] P. F. Faure and S. Rodts. *Proton NMR relaxation as a probe for setting cement pastes.* Journal of Magnetic Resonance Imaging, 26, pp. 1183-1193 (2008).

[48] Y. Q. Song, L. Venkataramanan, M. D. Hürlimann, M. Flaum, P. Frulla, C. Straley. *T_1–T_2 Correlation Spectra Obtained Using a Fast Two-Dimensional Laplace Inversion*. Journal of Magnetic Resonance, 154 (2), pp. 261-268 (2002).

[49] L. Rostom, D. Courtier-Murias, S. Rodts and S. Care. *Investigation of the effect of aging on wood hygroscopicity by 2D ^{1}H NMR relaxometry.* Holzforschung, 74 (4)**,** pp. 400-411 (2020).

[50] L. Rostom, S. Caré and D. Courtier-Murias. *Analysis of water content in wood material through 1D and 2D ^{1}H NMR relaxometry: Application to the determination of the dry mass of wood*. Magnetic Resonance in Chemistry, 59, pp. 614–627 (2021).

[51] A. Abragam. *The Principles of Nuclear Magnetism*. Clarendon Press, Oxford (1961).

[52] H. Knicker. *Solid state CPMAS ^{13}C and ^{15}N NMR spectroscopy in organic geochemistry and how spin dynamics can either aggravate or improve spectra interpretation*. Organic Geochemistry, 42, pp. 867–890 (2011).

[53] D. Courtier-Murias. *Potential and Application of Magnetic Resonance Imaging and relaxometry in Environmental Research*. eMagRes, 8, pp. 1–12 (2019).

[54] Y. Wang, M. B. Villamil, P. C. Davidson, N. Akdeniz. *Review: A quantitative understanding of the role of co-composted biochar in plant growth using meta-analysis.* Science of the Total Environment, 685, pp. 741-752 (2019).

[55] P. Godlewska, H. P. Schmidt, Y. S. Ok, P. Oleszczuk. *Biochar for composting improvement and contaminants reduction. A review.* Bioresource Technology, 246, pp. 193-202 (2017).

[56] G. Haider, S. Joseph, D. Steffens, C. Müller, S. Taherymoosavi, D. Mitchell, C. I. Kammann. *Mineral nitrogen captured in field-aged biochar is plant-available.* Scientific Reports, 10, nº 13816 (2020).

[57] J. M. De la Rosa, A. Z. Miller and H. Knicker. *Soil-borne fungi challenge the concept of long-term biochemical recalcitrance of pyrochar*. Scientific Reports, 8, nº 2896 (2018).

[58] Z. Liu, N. Qi, Y. Luan and X. Sun. *Thermogravimetry-Infrared Spectroscopy Analysis of the Pyrolysis of Willow Leaves, Stems and branches.* Advances in Material Science and Engineering, nº 303212 (2015).

[59] T. Carballo, M. V. Gil, X. Gómez and F. González-Andrés. *Characterization of different compost extracts using Fourier-transform infrared spectroscopy (FTIR) and thermal analysis.* Biodegradation, 19 (6), pp. 815-30 (2008).

[60] W. Braida, J. J. Pignatello, Y. Lu and P. Ravicovitch. *Sorption Hysteresis of Benzene in Charcoal Particles.* Environmental Science and Technology, 37 (2), pp. 409-17 (2003).

[61] V. Gargiulo, A. Gomis-Berenguer, P. Giudicciani and C. O. Ania. *Assessing the Potential of Biochars prepared by Steam-Assisted Slow Pyrolysis for CO_2 Adsorption and Separation*. Energy & Fuels, 32 (10), p. 10218 (2018).

[62] M. Zhou, S. Caré, D. Courtier‐Murias, P. Faure, S. Rodts and P. Coussot. *Magnetic resonance imaging evidences of the impact of water sorption on hardwood capillary imbibition dynamics*. Wood Science and Technology, Springer Verlag, 52 (4), pp. 929-955 (2018).

[63] D. J. Greenland. *Soil damage by intensive arable cultivation: temporary or permanent?* Philosophical transactions of the Royal Society B, 281 (980), pp. 193-208 (1977).